Editors' Suggestion

Finding the Ultranarrow $^3P_2 \rightarrow {}^3P_0$ Electric Quadrupole Transition in Ni^{12+} Ion for an Optical Clock

Charles Cheung,[1] Sergey G. Porsev,[1] Dmytro Filin,[1] Marianna S. Safronova,[1] Malte Wehrheim,[2,*] Lukas J. Spieß,[2] Shuying Chen,[2] Alexander Wilzewski,[2] José R. Crespo López-Urrutia,[3] and Piet O. Schmidt[2,4,†]

[1]*Department of Physics and Astronomy, University of Delaware, Newark, Delaware 19716, USA*
[2]*Physikalisch-Technische Bundesanstalt, Bundesallee 100, 38116 Braunschweig, Germany*
[3]*Max-Planck-Institut für Kernphysik, Saupfercheckweg 1, 69117 Heidelberg, Germany*
[4]*Institut für Quantenoptik, Leibniz Universitt Hannover, Welfengarten 1, 30167 Hannover, Germany*

(Received 19 February 2025; revised 3 June 2025; accepted 17 July 2025; published 28 August 2025)

The Ni^{12+} ion features an electronic transition with a natural width of only 8 mHz, allowing for a highly stable optical clock. We predict that the energy of this strongly forbidden $3s^2 3p^4\ {}^3P_2 \rightarrow 3s^2 3p^4\ {}^3P_0$ electric quadrupole transition is 20 081(10) cm^{-1}. For this, we use both a hybrid approach combining configuration interaction with a coupled-cluster method and a pure configuration interaction calculation for the complete 16-electron system, ensuring convergence. The resulting very small theoretical uncertainty of only 0.05% allowed us to find the transition experimentally in a few hours, yielding an energy of 20 078.984(10) cm^{-1}. This level of agreement for a 16-electron system is unprecedented and qualifies our method for future calculations of many other complex atomic systems. While paving the way for a high-precision optical clock based on Ni^{12+}, our theory and code development will also enable better predictions for other highly charged ions and other complex atomic systems.

DOI: 10.1103/flwf-c2m1

Introduction—Highly charged ions (HCI) are very interesting for searches for physics beyond the standard model of elementary particles and interactions [1]. Several of their predicted optical transitions have some of the highest sensitivities to variations of the fine-structure constant and, accordingly, enhance the corresponding dark matter searches and tests of local position invariance [1–3]. Such optical transitions are laser accessible and can provide high-precision frequency standards in atomic clocks [1,4].

Developing highest-accuracy clocks based on HCI is motivated by their extreme atomic properties: a much lower sensitivity to external electromagnetic perturbations than singly charged ions or neutral atoms and a strong suppression of systematic frequency shifts, such as ac Stark, electric quadrupole, and higher-order magnetic field shifts and from blackbody radiation.

This new class of clocks was demonstrated in 2022 with the reported optical magnetic-dipole transition in Ar^{13+} with an evaluated systematic frequency uncertainty of 2.2×10^{-17}, comparable to current operating optical clocks [4,5]. Increasing this accuracy is unpractical with Ar^{13+} due to the relatively short lifetime of the excited state, limiting interrogation times and, accordingly, the statistical uncertainty of optical frequency comparisons due to quantum projection noise to $3.2 \times 10^{-14}/\sqrt{\tau}$. Operating a clock with this stability would require an averaging time τ of 2 000 000 s to reach its systematic uncertainty and more than 30 years to average to 10^{-18}. Thus, we have chosen the strongly forbidden $3s^2 3p^4\ {}^3P_2 \rightarrow 3s^2 3p^4\ {}^3P_0$ electric quadrupole clock transition in Ni^{12+} [6] as the most suitable candidate for the next HCI clock, with a convenient wavelength, narrow transition, and relatively simple electronic structure. Its dominant systematic effects, such as electric quadrupole and second-order Zeeman shifts, are expected to be similarly small as for Ar^{13+} but have to be verified experimentally.

The main obstacle here was the large uncertainty of the clock state excitation energy of 0.5% (100 cm^{-1} or 3 THz), which would have required long scan times to find the extremely weak transition, which has a linewidth of only 8 mHz. In contrast, the wavelength of the $^3P_2 \rightarrow {}^3P_1$ $M1$ transition could be measured in emission due to its higher transition rate, resulting in a more accurate value [7] of 19 541.758(18) cm^{-1}. In addition, two more energy levels of the same configuration are reasonably well known and serve as computational benchmarks. In this Letter, we show how the problem is solved with a uniquely precise computation of Ni^{12+} low-lying energies with an uncertainty below 10 cm^{-1}, unprecedented for such a complicated atomic system. Applying recently developed fast laser frequency scanning techniques [8], our prediction allowed us to locate the sought-after transition within just

*Contact author: malte.wehrheim@quantummetrology.de
†Contact author: piet.schmidt@quantummetrology.de

one day at $20078.984 \pm 0.010\ \mathrm{cm}^{-1}$, only $2\ \mathrm{cm}^{-1}$ away from it. his comprises the first direct excitation of a transition in a highly charged ion without previous emission measurements in hot plasmas, as were available in the previously measured HCI clock candidates Ar^{13+} [4,9,10] and Ca^{14+} [11,12]. Our Letter has, thus, paved the way for the development of the Ni^{12+} clock and demonstrates the reliability of future calculations needed for the search of other clock transitions in HCI.

Theory: CI + all-order method—Ni^{12+} has 16 electrons in its ground state $1s^22s^22p^63s^23p^4$ configuration. We start with a hybrid approach that combines the configuration interaction (CI) method with the linearized coupled-cluster single-double (all-order) method [13]. In our "CI + all-order" method, CI is used to treat the six outer $3s^23p^4$ electrons, which we consider to be valence electrons. To account for the correlations between the ten core $1s^22s^22p^6$ and valence electrons, we applied the coupled-cluster method as described in Ref. [13].

The CI wave function is obtained as a linear combination of all distinct states of a given angular momentum J and parity $\Psi_J = \sum_i c_i \Phi_i$. In the pure CI approach, the wave functions and energies of the low-lying states are obtained by solving the many-electron Schrödinger equation $H\Phi_n = E_n\Phi_n$ [14]. The CI + all-order approach incorporates core excitations in the CI method by defining an effective Hamiltonian $H_{\mathrm{eff}}(E) = H + \Sigma(E)$, where H is the Hamiltonian in the frozen-core approximation. The energy-dependent operator $\Sigma(E)$ is constructed using the coupled-cluster method to account for the virtual excitations of the ten core electrons [13].

The one-electron orbitals of the core shells were obtained by solving the Dirac-Hartree-Fock equations in the central field approximation using a V^{N-6} basis, where N is the number of electrons. The basis set was constructed on a radial grid using B splines, with 40 splines of order 7, constrained to a spherical cavity of radius $R = 7$ a.u. This included a total of seven partial waves ($l_{\max} = 6$) and orbitals with a principal quantum number n of up to 35. The Breit and Coulomb interactions were included on the same footing for constructing the basis set, which is large enough for the coupled-cluster computations to accurately generate the effective Hamiltonian.

We apply several approximations of increasing accuracy to construct the effective Hamiltonian: second-order many-body perturbation theory (MBPT), linearized coupled-cluster method with single and double excitations (LCCSD), and coupled-cluster method with single, double, and triple excitations (CCSDT). We find very small differences, from $-1\ \mathrm{cm}^{-1}$ for the $^3P_1$ state to $-10\ \mathrm{cm}^{-1}$ for the $^1S_0$ state between the CI + LCCSD and the CI + MBPT results, showing that all higher-order core-valence correlations are very small. The CCSDT method included nonlinear single and double terms and linear triple terms, which are small and are listed under the column "NL + Tr" in Table I.

The convergence of the six-electron CI calculation to an accuracy of a few cm^{-1} is a major computational challenge and had not been demonstrated prior to this Letter to our knowledge. We start with all possible single and double (SD) excitations from the $3s^23p^4$, $3s^23p^34p$, $3s3p^44s$, $3s3p^43d$, $3s^23p^23d^2$, and $3p^6$ reference configurations to $17spdfg$, which means that all orbitals with the principal quantum number up to $n = 17$ and the $spdfg$ partial waves were included. The resulting energies are listed in Table I in the column "$17spdfg$." We expand the basis set and increase the number of starting configurations until a numerical convergence is reached in all parameters of the CI calculation. The procedure for extending the basis set is illustrated in Fig. 1. We start from the six reference configurations mentioned above but perform SD excitations to growing sets of orbitals. First, we increase only the principal quantum number to $n = 29$ while keeping the maximum orbital angular momentum $l = 4$ (i.e., $spdfg$ partial waves). The resulting contributions listed in Table I show that convergence has been reached for the $spdfg$ partial waves, given a negligible ($\lesssim 0.01\%$) contribution of states with $n > 22$ for the $^3P_0$ and $^3P_1$ levels.

Next, in addition to all excitations previously included [16], we allow SD excitations to the orbitals of h, i, k, and l partial waves. We list the contributions of the h and i partial waves separately to illustrate their significance. CI computations typically include only the first few orbitals (e.g., $6-12h$) for higher partial waves. We unexpectedly found that this practice drastically underestimates their contribution. It turned out that most of the contributions

TABLE I. Contributions to the excitation energies of the low-lying states (in cm^{-1}) calculated using the CI + all-order method. See the main text for detailed explanations of all contributions. Experimental values are displayed in column "Expt. [7,15]." The last two columns display the difference between the theoretical and experimental values.

Configuration	17 $spdfg$	18–22 $spdfg$	23–29 $spdfg$	6–28 h	7–28 i	$l > 6$	Extra configurations	NL + Tr	TEI	QED	Total	Expt. [7,15]	Difference	Difference (%)
$3s^23p^4\ ^3P_1$	19 459	9	0	8	4	4	0	−3	16	50	19 547	19542	6	0.03%
$3s^23p^4\ ^3P_0$	20 114	−3	−1	−8	−4	−4	−5	−3	−34	33	20 086	20 060(100)		
$3s^23p^4\ ^1D_2$	47 441	−49	4	−98	−46	−40	−19	−2	−163	43	47 063	47 033	30	0.06%
$3s^23p^4\ ^1S_0$	98 686	−89	9	−134	−66	−64	−56	−8	−416	50	97 894	97 836	58	0.06%

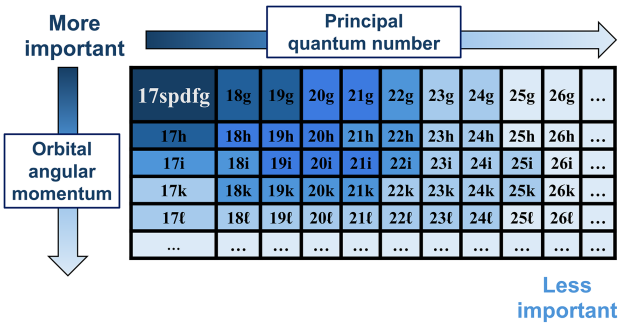

FIG. 1. Illustration of the basis set upscale. $17spdfg$ includes all orbitals up to $n = 17$ for $spdfg$ partial waves. Darker blocks indicate orbitals with larger contributions to the energies and wave functions.

from higher partial waves come from orbitals with higher principal quantum numbers. In fact, more than half of the contribution for the h partial wave comes from the (18–28) h orbitals in this basis set. This trend worsens for the i orbitals, where almost all of the contribution comes from $n > 17$. In the pure CI computation described below, we can partly remedy this issue by using a smaller, more compact basis built using a recurrent procedure with a better V^N potential. However, these orbitals lie very high in the spectrum, and excitations to orbitals with large n have to be included to ensure convergence. We extrapolated the contributions of the partial waves with $l > 6$ based on the convergence of energies for the h, i, k, and l partial waves. In Table I, we list the total contribution to the energies of higher partial waves in the column "$l > 6$."

Further significant contributions due to excitations from additional reference configurations are listed in column "extra configuration" in Table I. To select a new reference configuration, we order all configurations from the $17spdfg$ run by their weights and then extend the set of the reference configurations by adding those with the largest weight first. We first allow single excitations from 1200 reference configurations, then SD excitations from 41 more, and keep adding configurations until we reach convergence with good numerical accuracy. We note that CI convergence required a tremendous increase of the number of configurations: Single-double excitation to the $17spdfg$ orbitals produces 256 000 configurations; expanding the basis set to $28spdfgh$ yields another 933 000 configurations, while including i orbitals adds another 418 000 configurations. A total of 3.3 million extra configurations were included to obtain the result in column "extra configuration" These calculations became possible through improvements of the highly parallel pCI package [17,18] and separation of the total computations of more than 5 million configurations into a large number of manageable computations using PYTHON interfaces developed to automate this process.

We calculated QED corrections and three-electron interaction (TEI) corrections following Refs. [19,20], respectively, and listed them in columns "QED" and "TEI," respectively. The adequate (10% or better) accuracy of QED calculations has been established in Ref. [21]. TEI corrections are due to our separation of the computations into core and valence sectors and are not accounted for by the CI + all-order method. In column "total," we present the final energies, calculated by adding all corrections beyond the initial results $17spdfg$. In the last two columns in Table I, we show the small differences between our final CI + all-order values and the experimental results compiled in the National Institute of Standards and Technology [7,15] database of only 0.03% for the $^3P_1$ state and 0.06% for the $^1D_2$ and $^1S_0$ states, respectively.

Theory: Pure CI method—The largest uncertainty in the previous approach comes from interactions of four and more electrons that are omitted in the TEI-type correction. Their effect would be intrinsically included in the pure CI approach. Therefore, we now correlate all 16 electrons on the same footing within the CI instead of using the coupled-cluster effective Hamiltonian approach. The challenge now is that the number of configurations needed would require total and per-core memory resources beyond those commonly available at high-performance clusters. We have investigated different ways of efficiently breaking the CI computation to separate expansions yielding additive energy corrections that enabled us to perform this computation.

First, we form a smaller basis set using the recurrent procedure described in Refs. [14,22], because we no longer need the large basis used for coupled-cluster computations. This basis set is constructed in a more compact radial cavity of 5 a.u., which led to an accelerated convergence with the principal quantum number n. We start by allowing only SD excitations from the outer six electrons to $20spdfghikl$ orbitals and extrapolating for higher partial waves. These results are listed in the three columns labeled "six electrons" in Table II. We find that CI saturation was achieved already at $n = 17$, as the contribution of $n = 18$–20 was negligible ($\lesssim 0.01\%$) for all partial waves. Then, we allow additional SD excitations from the $1s$, $2s$, and $2p$ shells of the inner ten electrons to the $spdfg$ partial waves from the same dominant reference configurations (columns "all electrons" in Table II). We also verified that additional excitations of the inner ten electrons to the basis states in $l > 4$ partial waves gave a negligible contribution.

Next, we analyzed how energy levels change when we add excitations from additional reference configurations with the highest weights, which we select as in the CI + all-order approach described above (see column "extra configuration" in Table II).

In total, we computed contributions from 9.6 million configurations broken down into 54 separate computations, with our memory of 31 TB limiting the set size for each single run to roughly 350 000 configurations. This Letter prompted us to develop a neural-network-based algorithm that reduced memory needs and computation time by a

TABLE II. Contributions to the excitation energies of the low-lying states (in cm^{-1}) calculated using the 16-electron CI method. Results in the three columns labeled "six electrons" are obtained, allowing excitations from the last six electrons. In all other calculations labeled "all electrons," the excitations are allowed from all 16 electrons. See the text for detailed explanations of all contributions. Experimental values are displayed in column "Expt. [7,15].".

	Six electrons			All electrons								
Configuration	17 $spdfg$	17 $l>4$	18–20 $spdfghikl$	11 $spdfg$	12–18 $spdfg$	Extra configurations	Estimate full CI	QED	Total	Expt. [7,15]	Difference	Difference (%)
$3s^2 3p^4\ ^3P_1$	19 395	16	0	83	6	1	0	49	19 550	19 542	8	0.04%
$3s^2 3p^4\ ^3P_0$	20 052	−15	0	14	−5	5	−3	33	20 081	20 060(100)		
$3s^2 3p^4\ ^1D_2$	47 348	−179	−1	−105	−2	−45	−5	42	47 051	47 033	18	0.04%
$3s^2 3p^4\ ^1S_0$	98 397	−260	−4	−318	−110	38	−24	52	97 771	97 836	−66	−0.07%

factor of 3 and human involvement even more [23]. The network was trained to select the most important configurations more efficiently in an automated, iterative process. The essentially exact computations above confirmed these neural network results.

In addition, we estimate the contribution of all remaining configurations in the CI expansion, which is impossible to compute directly. We studied how the difference in weights of a configuration contributing to the excited and ground states affects the respective energy contribution if we consider this configuration as a reference one. We found a linear dependence (similar for all four levels) with a relative weight of 0.01% leading to a correction of about -11 cm^{-1}.

We tested this relation using contributions to the energies of configurations that were already computed. We added weights from 200, 2000, and 9500 additional reference configurations until convergence was reached and estimated the total contribution based on the above relation. We note that 9500 reference configurations would lead to probably billions of configurations in the CI expansion, making it completely untractable with any computational facilities. This contribution is listed in column "estimate full CI." To the best of our knowledge, such a quantitative estimate to complete CI has never been made before.

The QED corrections are listed in the column labeled "QED," and the final energies under column "total" are compared with the experimental values [7,15] displayed in the last two columns. The $^3P_0$ energies obtained by two approaches differ by only 5 cm^{-1}. The difference from the experiment for the $^3P_1$ state is 6 and 8 cm^{-1}. Based on this, we conservatively estimate the energy uncertainty for $^3P_0$ to be 10 cm^{-1}. We take the CI value 20081 ± 10 cm^{-1} to be final, since the convergence of the CI was demonstrated and all corrections except QED nearly cancel for the $^3P_0$ level.

Experiment: Finding the clock transition—Starting with this prediction, we experimentally searched for the $^3P_2 \rightarrow {}^3P_0$ clock transition in Ni^{12+}. For this, we produced HCI in an electron beam ion trap (EBIT) [24] and transported them to a cryogenic Paul trap [25], where we cotrapped one Ni^{12+} with a single Be^+ ion for sympathetic cooling and readout through its coupled motion using quantum-logic-inspired methods [10,26].

The uncertainty range of our calculation is 300 GHz (10 cm^{-1}) and can be scanned within one day of continuous operation using the methods introduced in Ref. [8]. In summary, we used our spectroscopy laser at 498 nm to drive excitations to the $^3P_0$ state, which were then detected by the absence of an excitation signal on the $^3P_2 \rightarrow {}^3P_1$ transition. For this, we first identified the $^3P_2 \rightarrow {}^3P_1$ transition using an off-resonant optical dipole force (ODF) [8]. The ODF arises from the two counterpropagating laser beams with frequencies $\omega_1 = \omega$ and $\omega_2 = \omega - \omega_m$, where ω_m is the characteristic motional frequency of the ions' in the trap. As the laser frequency ω approaches the electronic resonance ($\lesssim$10 MHz), the ion motion is coherently excited [8,27] without populating the electronically excited state $^3P_1$. The ensuing phonon excitation is detected with high efficiency through the Be^+ logic ion by mapping motional to spin excitation. The $^3P_2 \rightarrow {}^3P_1$ transition frequency is determined to be 585.847263 ± 0.000010 THz using a commercial wave meter calibrated with an iodine-stabilized laser at 626 nm. This result agrees well with the EBIT emission measurement [7] and the transition frequency calculated above.

In the search for the clock transition, we then used the motion induced by the ODF at a fixed detuning of 5 MHz from the $^3P_2 \rightarrow {}^3P_1$ stretched-state resonance as a signal that vanishes upon excitation of the $^3P_2 \rightarrow {}^3P_0$ clock transition. A frequency-doubled titanium-sapphire laser provided about 100 mW of power at 498 nm for this. We estimated an on-resonant Rabi frequency of 20 kHz and a specified laser linewidth of < 100 kHz averaged over 100μs. With these parameters, we estimated an optimal scanning speed of 1 GHz/s at 50 cycle repetitions, following Ref. [8] for this experiment. We expect a 20% excitation probability to the $^3P_0$ state when the laser frequency hits the transition during a scan. A search cycle consists of three phases. Initially, the $^3P_2$, $m_J = 2$ edge state is prepared by optical pumping (∼70%) on the $^3P_2 \rightarrow {}^3P_1$ transition, taking approximate 50 ms. In the second step, the HCI is

irradiated by the 498 nm laser, and the laser frequency is linearly swept over a span of 5 GHz in 5 s. Finally, the population of the ground state is read out by interrogating the $^3P_2 \rightarrow {}^3P_1$ transition with the ODF described above. The last readout step is repeated 70 times to utilize the experimental dead time of 2 s needed to reset the laser to its sweeping starting frequency. This quantum nondemolition detection scheme [28] allowed us to detect the excitation from the ground state with nearly 100% fidelity. In total, we covered in six hours 100 GHz within the uncertainty range until we found the clock transition. Figure 2 shows an example of an off-resonant clock-laser scan leading to high motional excitation by the ODF (blue dots), as well as the motional detection background (orange dots). The shaded color bands cover the region of the mean of the excitation probability and their standard deviations. The green points show excitation signals when scanning across the clock transition and within the background and motional excitation bands provide a clear signature of the clock-transition excitation. We observe detection events between the detection bands due to excitation to the clock state and subsequent deexcitation to different Zeeman substates within one scan. This can arise from the laser crossing motional and micromotion sidebands during the remainder of the scan, as well as spontaneous decay after initial excitation. The resulting change in common detuning of the readout laser to the $^3P_1$ transition leads to a reduction of the ODF readout signal. For a more precise measurement, we narrowed the scanning range to 300 MHz, which is our uncertainty from drifts of the not-stabilized titanium-sapphire laser. We determined the $^3P_2 \rightarrow {}^3P_0$ clock-transition frequency at 601.9528 ± 0.0003 THz

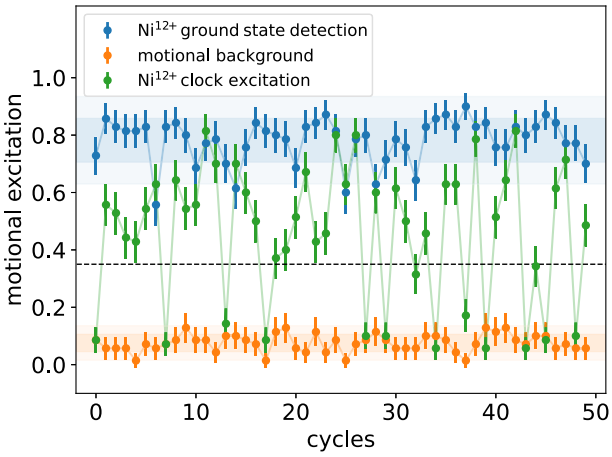

FIG. 2. Measurement of the motional excitation after the $^3P_2 \rightarrow {}^3P_0$ laser scan. Motional background (orange) and motional excitation (blue) are clearly separated, allowing one to threshold the data (black dashed line) for state detection. Scanning across the clock transition resonance frequency (green) leads to repeated quantum jumps appearing in both detection bands (shaded areas) in different scanning cycles. Error bars on the data points display the quantum projection noise from 70 repetitions.

[20078.984 ± 0.010 cm^{-1}] with our wave meter, in excellent agreement with the theory prediction. Future frequency stabilization of the laser to hertz-level linewidth will allow us to perform quantum logic spectroscopy [10] and operate an optical clock based on Ni^{12+}.

Conclusion—We predicted the $^3P_2$-$^3P_0$ transition energy using two different theoretical approaches, demonstrating full convergence of a 16-electron CI computation including 9.6 million configurations and developed a method to estimate the residual contributions of the far more numerous configurations that cannot be realistically included in existing computer clusters. This Letter demonstrates how our advanced theory and code development lead to much smaller calculational uncertainties. Our optimized parallel code package has been made available to the community [18]. We demonstrated its ability to include millions of configurations by effectively separating different classes of excitations. Our subsequent development of automated neural network tools further reduces the use of memory and computation time [23]. The method and code development from this Letter can be used to constrain uncertainties in future calculations of other complex atoms and ions.

The subsequent experiment demonstrated excitation of this clock transition at 20078.984 ± 0.010 cm^{-1}, just 2 cm^{-1} away from the prediction. This remarkable agreement with the *ab initio* calculations of a 16-electron system inspires confidence in future calculations of other complex atomic systems and enables the further development of a Ni^{12+} high-precision atomic clock.

Acknowledgments—We thank Mikhail Kozlov for the helpful discussion of the calculations and Pavlo Bilous for his collaboration on integrating neural network support into CI calculations. We thank Thomas Legero for mounting the mirrors of our 1024 nm stabilization cavity. The project was supported by the Physikalisch-Technische Bundesanstalt, the Max-Planck Society, Max-Planck-RIKEN-PTB-Center for Time, Constants and Fundamental Symmetries, and the Deutsche Forschungsgemeinschaft (DFG, German Research Foundation) through SCHM2678/5-2, the collaborative research centers SFB 1225 ISOQUANT and SFB 1227 DQ-*mat*, and under Germany's Excellence Strategy EXC-2123 QuantumFrontiers 390837967. This project 20FUN01 TSCAC has received funding from the EMPIR programme co-financed by the Participating States and from the European Union's Horizon 2020 research and innovation programme. This project has received funding from the European Research Council (ERC) under the European Unions Horizon 2020 research and innovation program (Grant Agreement No. 101019987). The calculations in this work were done through the use of information technologies resources at the University of Delaware, specifically the high-performance Caviness and DARWIN computer clusters. The theoretical work has been supported in part by the U.S. NSF Grant

No. PHY-2309254, U.S. Office of Naval Research Grants No. N000142012513 and No. N000142512105, and by the European Research Council (ERC) under the Horizon 2020 Research and Innovation Program of the European Union (Grant Agreement No. 856415).

Data availability—The data that support the findings of this article are openly available [29].

[1] M. G. Kozlov, M. S. Safronova, J. R. Crespo López-Urrutia, and P. O. Schmidt, Rev. Mod. Phys. **90**, 045005 (2018).
[2] M. S. Safronova, D. Budker, D. DeMille, D. F. J. Kimball, A. Derevianko, and C. W. Clark, Rev. Mod. Phys. **90**, 025008 (2018).
[3] R. Shaniv, R. Ozeri, M. S. Safronova, S. G. Porsev, V. A. Dzuba, V. V. Flambaum, and H. Häffner, Phys. Rev. Lett. **120**, 103202 (2018).
[4] S. A. King, L. J. Spieß, P. Micke, A. Wilzewski, T. Leopold, E. Benkler, R. Lange, N. Huntemann, A. Surzhykov, V. A. Yerokhin, J. R. Crespo López-Urrutia, and P. O. Schmidt, Nature (London) **611**, 43 (2022).
[5] A. D. Ludlow, M. M. Boyd, J. Ye, E. Peik, and P. O. Schmidt, Rev. Mod. Phys. **87**, 637 (2015).
[6] Y.-m. Yu and B. K. Sahoo, Phys. Rev. A **97**, 041403(R) (2018).
[7] S. Chen, Z. Zhou, J. Li, T. Zhang, C. Li, T. Shi, Y. Huang, K. Gao, and H. Guan, Phys. Rev. Res. **6**, 013030 (2024).
[8] S. Chen, L. J. Spieß, A. Wilzewski, M. Wehrheim, K. Dietze, I. Vybornyi, K. Hammerer, J. R. Crespo López-Urrutia, and P. O. Schmidt, Phys. Rev. Appl. **22**, 054059 (2024).
[9] R. Soria Orts, Z. Harman, J. R. Crespo López-Urrutia, A. N. Artemyev, H. Bruhns, A. J. González Martínez, U. D. Jentschura, C. H. Keitel, A. Lapierre, V. Mironov, V. M. Shabaev, H. Tawara, I. I. Tupitsyn, J. Ullrich, and A. V. Volotka, Phys. Rev. Lett. **97**, 103002 (2006).
[10] P. Micke, T. Leopold, S. A. King, E. Benkler, L. J. Spiess, L. Schmöger, M. Schwarz, J. R. Crespo López-Urrutia, and P. O. Schmidt, Nature (London) **578**, 60 (2020).
[11] N.-H. Rehbehn, M. K. Rosner, H. Bekker, J. C. Berengut, P. O. Schmidt, S. A. King, P. Micke, M. F. Gu, R. Müller, A. Surzhykov, and J. R. Crespo López-Urrutia, Phys. Rev. A **103**, L040801 (2021).
[12] A. Wilzewski *et al.*, Phys. Rev. Lett. **134**, 233002 (2025).
[13] M. S. Safronova, M. G. Kozlov, W. R. Johnson, and D. Jiang, Phys. Rev. A **80**, 012516 (2009).
[14] M. G. Kozlov, S. G. Porsev, and V. V. Flambaum, J. Phys. B **29**, 689 (1996).
[15] A. Kramida, Yu. Ralchenko, J. Reader, and and NIST ASD Team, NIST Atomic Spectra Database (ver. 5.9), [Online]. Available: https://physics.nist.gov/asd [Mon Jun 20 2022]. National Institute of Standards and Technology, Gaithersburg, MD (2022).
[16] We find the calculations of k and l partial waves to be intractable with such a large basis. We have verified with h and i partial waves that, as expected, the total contribution of a partial wave does not depend on the choice of the basis. We use far more compact basis with the pure CI method to compute the contributions of k and l for partial waves.
[17] C. Cheung, M. S. Safronova, and S. G. Porsev, Symmetry **13**, 621 (2021).
[18] C. Cheung, M. G. Kozlov, S. G. Porsev, M. S. Safronova, I. I. Tupitsyn, and A. I. Bondarev, Comput. Phys. Commun. **308**, 109463 (2025).
[19] I. I. Tupitsyn, M. G. Kozlov, M. S. Safronova, V. M. Shabaev, and V. A. Dzuba, Phys. Rev. Lett. **117**, 253001 (2016).
[20] M. G. Kozlov, M. S. Safronova, S. G. Porsev, and I. I. Tupitsyn, Phys. Rev. A **94**, 032512 (2016).
[21] C. Shah, M. Togawa, M. Botz, J. Danisch, J. J. Goes, S. Bernitt, M. Maxton, K. Köbnick, J. Buck, J. Seltmann, M. Hoesch, M. F. Gu, F. S. Porter, T. Pfeifer, M. A. Leutenegger, C. Cheung, M. S. Safronova, and J. R. Crespo López-Urrutia, Astrophys. J. **969**, 52 (2024).
[22] M. G. Kozlov, S. G. Porsev, M. S. Safronova, and I. I. Tupitsyn, Comput. Phys. Commun. **195**, 199 (2015).
[23] P. Bilous, C. Cheung, and M. Safronova, Phys. Rev. A **110**, 042818 (2024).
[24] P. Micke, S. Kühn, L. Buchauer, J. R. Harries, T. M. Bücking, K. Blaum, A. Cieluch, A. Egl, D. Hollain, S. Kraemer, T. Pfeifer, P. O. Schmidt, R. X. Schüssler, C. Schweiger, T. Stöhlker, S. Sturm, R. N. Wolf, S. Bernitt, and J. R. Crespo López-Urrutia, Rev. Sci. Instrum. **89**, 063109 (2018).
[25] T. Leopold, S. A. King, P. Micke, A. Bautista-Salvador, J. C. Heip, C. Ospelkaus, J. R. Crespo López-Urrutia, and P. O. Schmidt, Rev. Sci. Instrum. **90**, 073201 (2019).
[26] P. O. Schmidt, T. Rosenband, C. Langer, W. M. Itano, J. C. Bergquist, and D. J. Wineland, Science **309**, 749 (2005).
[27] F. Wolf, Y. Wan, J. C. Heip, F. Gebert, C. Shi, and P. O. Schmidt, Nature (London) **530**, 457 (2016).
[28] D. B. Hume, T. Rosenband, and D. J. Wineland, Phys. Rev. Lett. **99**, 120502 (2007).
[29] M. Wehrheim, L. J. Spieß, S. Chen, A. Wilzewski, and P. Schmidt, Experimental data for figure 2 in "Finding the ultra-narrow 3P2 → 3P0 electric quadrupole transition in Ni12+ ion for an optical clock". Zenodo (2025), 10.5281/zenodo.16900465.